Hindawi
Advances in Civil Engineering
Volume 2020, Article ID 7302141, 15 pages
https://doi.org/10.1155/2020/7302141

Research Article

Improved Nonlinear Nishihara Shear Creep Model with Variable Parameters for Rock-Like Materials

Hang Lin[1], **Xing Zhang**[1], **Yixian Wang**[2], **Rui Yong**[3], **Xiang Fan**[4], **Shigui Du**[3] and **Yanlin Zhao**[5]

[1]*School of Resources and Safety Engineering, Central South University, Changsha, Hunan 410083, China*
[2]*School of Civil Engineering, Hefei University of Technology, Hefei 230009, China*
[3]*Ocean College, Zhejiang University, Zhoushan, Zhejiang 316000, China*
[4]*School of Highway, Chang'an University, Xi'an, Shannxi 710064, China*
[5]*School of Energy and Safety Engineering, Hunan University of Science and Technology, Xiangtan, Hunan 411201, China*

Correspondence should be addressed to Yixian Wang; wangyixian2012@hfut.edu.cn

Received 19 September 2019; Revised 13 January 2020; Accepted 3 February 2020; Published 27 February 2020

Academic Editor: Flavio Stochino

Creep property is an important mechanical property of rocks. Given the complexity of rock masses, mechanical parameters change with time in the creep process. In this work, a nonlinear function for describing the time-dependent change of parameters was introduced and an improved variable-parameter nonlinear Nishihara shear creep model of rocks was established. By creating rock-like materials, the mechanical properties of rocks under the shear creep test condition were studied, and the deformation characteristics and long-term shear strength of rocks during creep were analyzed. The material parameters of the model were identified using the creep test results. Comparison of the model's calculated values and experimental data indicated that the model can describe the creep characteristics of rocks well, thus proving the correctness and rationality of the improved model. During shear creep, the mechanical properties of rocks have an aging effect and show hardening characteristics under low shear stress. Furthermore, according to the fact that G_k of the nonlinear model can characterize the creep deformation resistance, a method to determine the long-term shear strength is proposed.

1. Introduction

Creep property is an important mechanical property of rocks and the main factor affecting long-term stability of geotechnical engineering [1–7]. Obtaining the stress and deformation characteristics of rock masses from the perspective and method of their rheology is consistent with reality [8–10]. Thus, studying the creep characteristics of rocks is crucial. The creep behavior of rocks can be divided into three stages, namely, attenuated, stable, and accelerated creep. In the initial creep stage, the strain increases with time. In the steady-state creep stage, the strain increases uniformly with time, and the duration of this stage is relatively long. In the accelerated creep stage, the strain rate increases with time, and the rock is destroyed after reaching the critical fracture point. Numerous studies have shown that rocks exhibit typical nonlinear characteristics during creep, in which the accelerated creep stage is the most obvious [4, 11, 12]. To reveal the mechanical properties of rock rheological behavior, scholars have conducted targeted in-depth research and obtained abundant research results [13–15]. By summarizing existing rheological models, Xia et al. [16] proposed a unified rheological mechanical model. Relevant studies have shown that model parameters vary during rock creep and are related to stress, time, temperature, and other factors [17, 18]. Referring to damage mechanics theory [19, 20], Jia et al. [21] proposed a nonlinear elastic-viscoplastic damage model based on the modified Mohr–Coulomb criterion. Moghadamaab [22] used -constitutive model to describe expansion and short- and long-term damages in the creep process of rock salt and established a numerical model of the rock salt excavation

underground chamber as it changes with time. Yang and Li [11] replaced the viscous element of the Nishihara model with a new element by using fractional calculus and established a nonlinear Nishihara model that describes rock rheology. Shao et al. [23] established a full stress-strain creep model from the perspective of microstructure evolution by considering various factors. These models effectively describe the nonlinear characteristics of model parameters during rock creep but focus on the creep mechanical properties of rocks under uniaxial and triaxial compression. Research on rock characteristics under direct shear creep conditions is relatively scarce. The primary failure mode of rocks under natural conditions is shear failure [24–30]. Therefore, the shear creep failure behavior of rocks should be studied. The classical Nishihara model can describe the mechanical properties of rocks in decay and stable creep stages [11, 31, 32], but its parameters are constant and cannot reflect the nonlinear characteristics of creep. To reveal the mechanism of rock mechanical behavior under shear creep conditions and establish a corresponding shear creep model, this study investigated the shear rheological mechanical characteristics of rocks with plastic-elastic deformation by performing a shear test on a similar sandstone material. A time-varying factor was introduced to the Nishihara model to describe the functional relationship between the viscosity coefficient and time. On the basis of this factor, an improved nonlinear Nishihara shear creep model that can reveal the unsteady and nonlinear characteristics of parameters was established. The model's rationality was verified through a comparison with experimental values.

2. Specimen Preparation and Test Methods

Natural rock masses contain many micro- and macrocracks, which lead to different physical and mechanical characteristics [33–41]. Miller divided the stress-strain curves of rocks with different physical and mechanical properties into six categories [42, 43]. The third category is called the plastic-elastic deformation feature, in which the stress-strain curve is concave in the initial stage and then becomes a straight-line segment until destruction [44–46]. Rocks with many pores and microfractures, such as granite and sandstone, reflect this deformation characteristic [47, 48]. In this study, the mechanical behavior and deformation characteristics under shear creep conditions were studied by fabricating similar materials with the plastic-elastic deformation feature of rocks [49].

Experiments were performed on a RYL-600 computer-controlled rock shear rheometer, which is usually used for rheological testing of materials, such as rock and concrete, and composed of three components: the host, the test and control system, and the computer system. The rheometer can simultaneously apply vertical-axis compression test force and horizontal-axis shear test force to a specimen and control the loading by force or deformation. In the shear creep test, the rock-like specimens were under constant temperature and humidity conditions. The loading rate at each stage was 300 N/s. The specimens adopted the same type of material, mix ratio, curing time, and mold specification ($10\ \text{cm} \times 10\ \text{cm} \times 10\ \text{cm}$). Through the uniaxial and triaxial compression tests, the mechanical parameters of rock materials with different cement, river sand, and water ratio were obtained. Finally, the sandstone materials with cement, river sand, and water ratio of 1 : 1 : 0.406 were selected as research objects. The mechanical parameters of the rock-like specimens are shown in Table 1, which is similar to the mechanical properties of sandstones with elastoplastic deformation characteristics. During pouring, the material was mixed according to the ratio, and the surface was smoothed after tamping in the steel mold to minimize adverse effects in the manufacturing process. The mold was taken apart after modeling for 24 hours and maintained for 28 days. All specimens are intact rock-like materials.

As the loading model shown in Figure 1, the specimens were subjected to a fast shear test to compare the strength characteristics of the rock's fast shearing and shear creep conditions. The test results are shown in Figure 2. At the beginning of loading, the slope of the stress-strain curve increased with the loading stress, and this process lasted for a long time. After the microcracks were compacted completely, the slope of the curve entered the linear elastic stage with a constant size and then maintained this feature until failure. Significant plastic elastic deformation characteristics were exhibited. The fast shear strengths of specimens 1–4 were 4.1 MPa, 5.6 MPa, 6.45 MPa, and 7.33 MPa, respectively. In the grading loading creep test, normal stress was taken as 5%, 10%, 15%, and 20% of the uniaxial compressive strength of a specimen. The shear stress levels of specimen 1 were 30%, 40%, 50%, 60%, and 70% of the fast shear strength. The shear stress levels of specimen 2 were 30%, 40%, 50%, and 60% of the fast shear strength until destruction. The shear stress levels of specimen 3 were 30%, 40%, 60%, 70%, and 80% of the fast shear strength. The shear stress levels of specimen 4 were 30%, 50%, 60%, 70%, and 80% of the fast shear strength. The loading method is presented in Table 2, and the process is shown in Figure 3.

3. Test Results and Analysis

3.1. Mechanical Properties with Time. The creep curves of graded shear loading under the same normal stress level were obtained through the creep shear test (Figure 4). In the creep test curve obtained, a straight line parallel to the longitudinal axis was made to intersect with the creep curve under the same normal stress and different shear forces, and the isochronal curve (Figure 5) was drawn by the stress and displacement values at each intersection point obtained. As can be seen from Figure 5, the slope of the isochronous shear stress-shear displacement curve varies with stress. Stress is the factor that affects the mechanical properties of rocks with plastic-elastic deformation characteristics, which are different from the characteristics of the microfracture compaction stage completed immediately after loading in most rocks. To study the time deterioration effect on the rock creep process, the deformation modulus under different creep time conditions was calculated through the slope of the curve section of the adjacent shear stress levels, and the

Table 1: The mechanical parameters of the rock-like specimens.

Parameter	σ_c (MPa)	μ	φ (°)	c (MPa)
Specimen	15.6	0.21	60	3.12

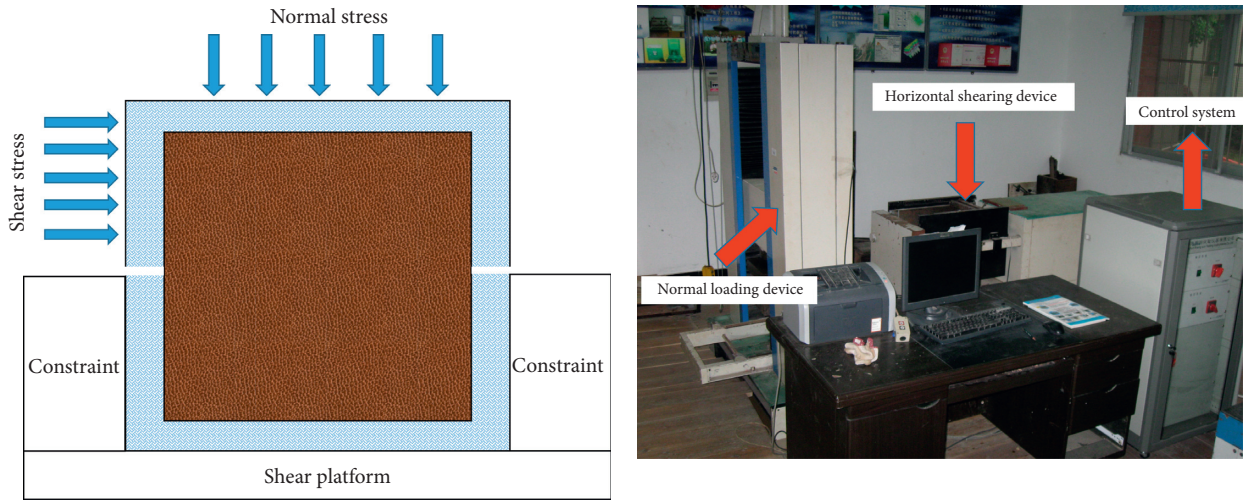

Figure 1: (a) Specimen loading model and (b) test equipment diagram.

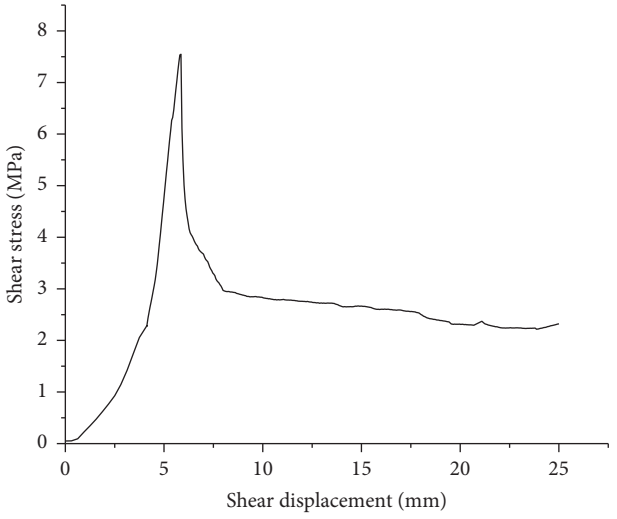

Figure 2: Shear stress-shear displacement relationship in the fast shear test under 3.12 MPa normal stress.

Table 2: Test grading loading method.

Specimen number	Normal stress (MPa)	Shear strength (MPa)	Shear stress (MPa)				
			1	2	3	4	5
1	0.78	4.1	1.23	1.64	2.05	2.46	2.87
2	1.56	5.6	1.68	2.24	2.8	3.36	Broken
3	2.34	6.45	1.935	2.58	3.87	4.515	5.16
4	3.12	7.33	2.199	3.665	4.398	5.131	5.864

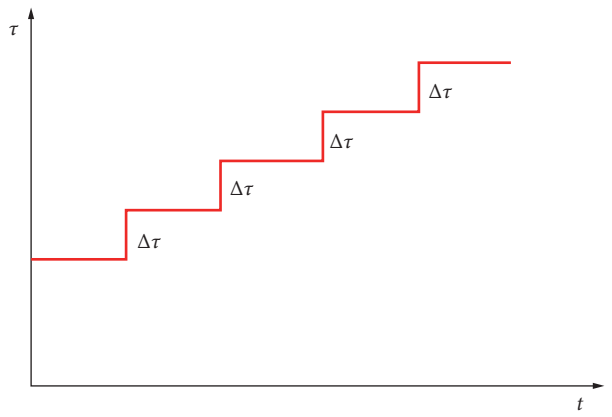

Figure 3: Schematic diagram of grading loading process.

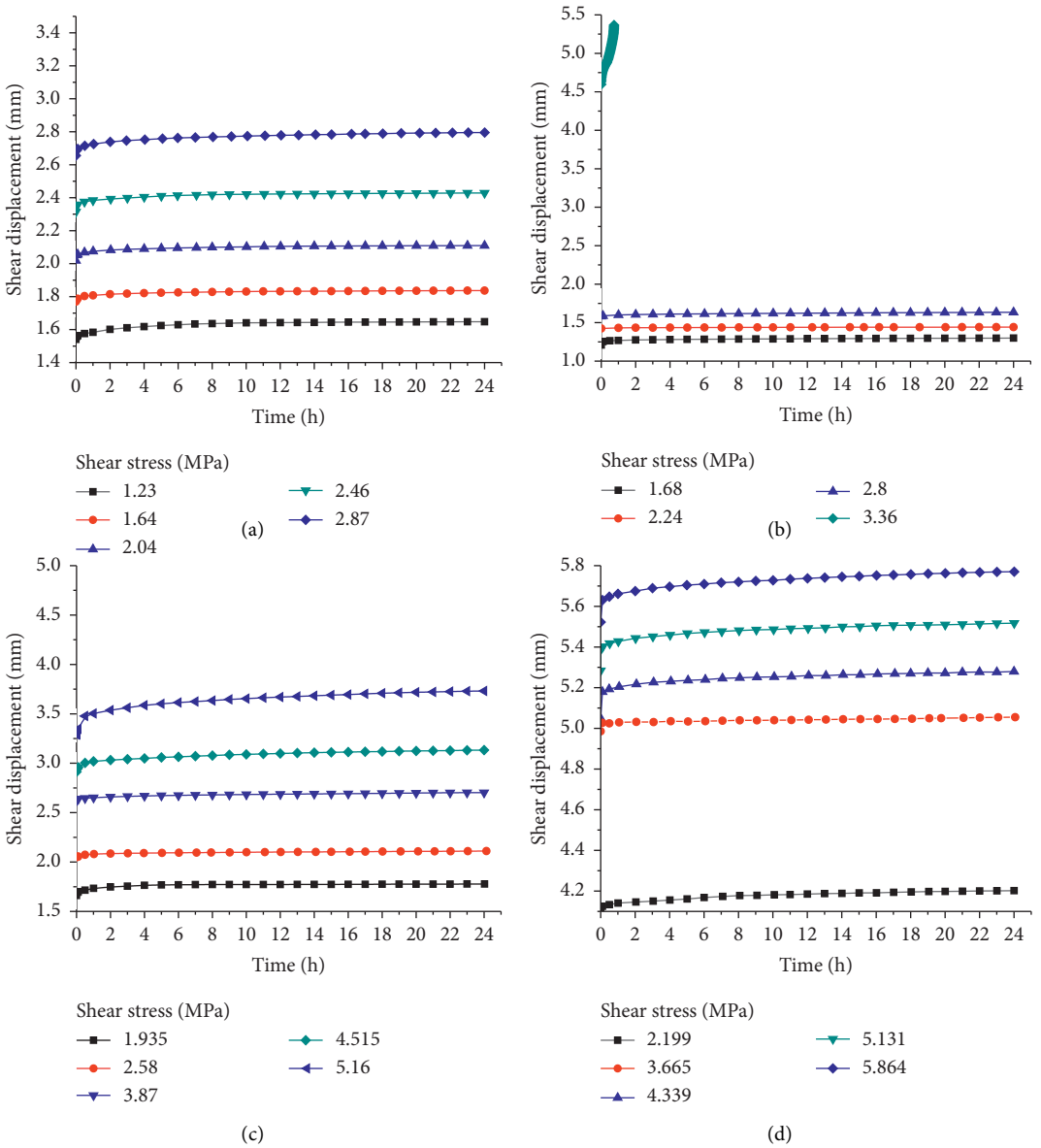

Figure 4: Shear displacement-time curves under different normal stresses: (a) 0.78 MPa, (b) 1.56 MPa, (c) 2.34 MPa, and (d) 3.12 MPa.

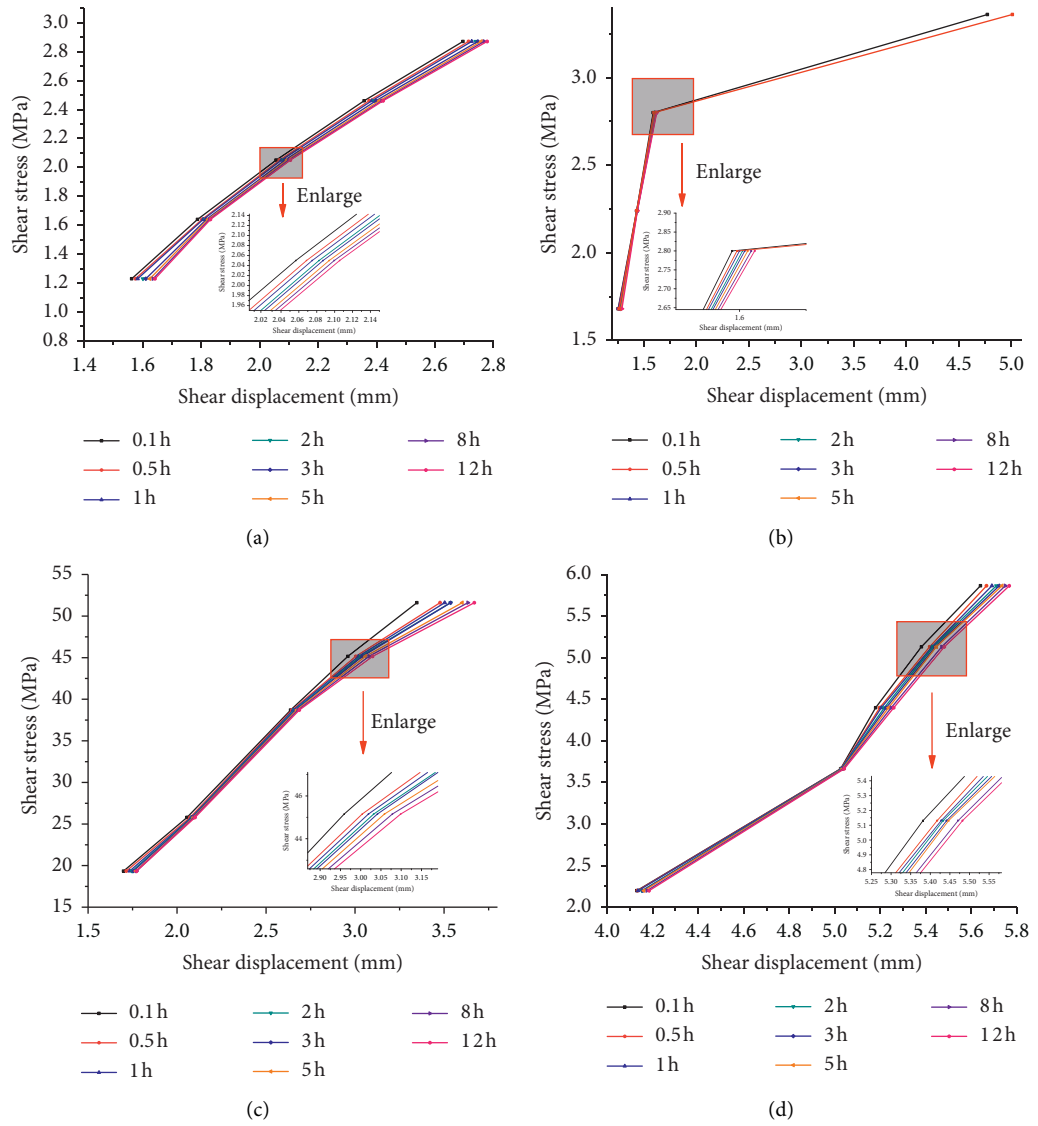

Figure 5: Isochronal graphs under different normal stresses: (a) 0.78 MPa, (b) 1.56 MPa, (c) 2.34 MPa, and (d) 3.12 MPa.

relationship between deformation modulus and time was plotted and is shown in Figure 6.

The formula for calculating the deformation modulus can be written as

$$E = \frac{\tau_1 - \tau_2}{\gamma_{\tau_1}^t - \gamma_{\tau_2}^t}, \tag{1}$$

where τ_1 and τ_2 characterize the adjacent two-stage shear stress and $\gamma_{\tau_1}^t$ and $\gamma_{\tau_2}^t$ indicate the shear displacement at different moments under the respective shear stress conditions.

Figure 6 indicates that for the rocks with plastic-elastic deformation characteristics, under the condition of low shear stress, the deformation modulus of rocks in creep behavior increased with time, which is contrary to the deterioration of the mechanical properties of most rocks with time [50, 51]. This result is due to the existence of many microcracks in plastic-elastic rocks [52, 53]. Low shear stress cannot easily compact the microcracks inside the rock completely in a short time, and the microcracks that are not compacted continue to be compacted in the following creep behavior, thus showing a hardening effect. When the shear stress level was increased to a certain value, the deformation modulus weakened with time and showed aging deterioration. This phenomenon occurred because the shear stress at this time exceeded the critical shear stress when the microcrack was completely compacted, which not only stopped the hardening effect brought by microcrack compaction but also developed the internal crack of the specimen with time and produced significant aging degradation effects. When the shear stress continues to increase, the mechanical properties of the rock continued to deteriorate with time because the unfinished area of the rock when shear stress was applied to the upper stage continued to deteriorate under the new first-order shear stress condition. Meanwhile, the increase in shear stress led to the deterioration of the area that is not easy to deteriorate under the condition of the shear stress of the upper level, resulting in continuous internal damage of the specimen.

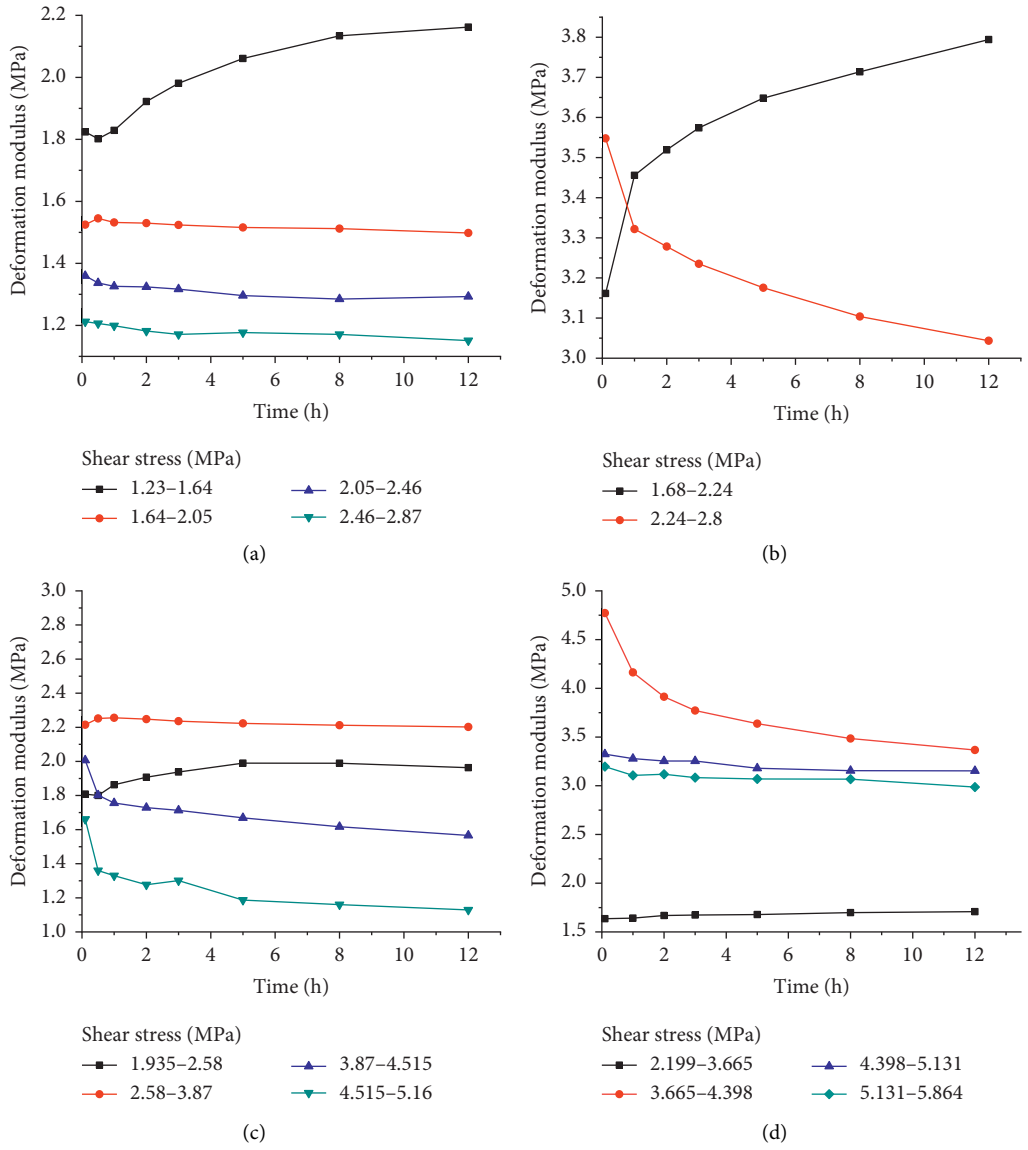

Figure 6: Deformation modulus-time diagrams under different normal stresses: (a) 0.78 MPa, (b) 1.56 MPa, (c) 2.34 MPa, and (d) 3.12 MPa.

3.2. Determination of Long-Term Strength under Different Normal Stress Conditions. According to the isochronous curve method which is commonly used in rheological mechanics [54], the stress corresponding to the second turning point of the isochronous curve after the fully compacted linear elastic phase was used as the long-term strength value of the rock. In Figures 5(a)–5(d), the shear stress value corresponding to the second turning point is 2.04 MPa, 2.8 MPa, 4.515 MPa, and 5.131 MPa, respectively. Thus, the long-term shear strength of the specimen under the normal stress condition of 0.78 MPa, 1.56 MPa, 2.34 MPa, and 3.12 MPa is 2.04 MPa, 2.8 MPa, 4.515 MPa, and 5.131 MPa, respectively. Correspondingly, the ratio of long-term shear strength to fast shear strength is 0.5, 0.5, 0.7, and 0.702, respectively. The phenomenon wherein the specimen had different ratios of long-term strength to fast shear strength under different normal stress conditions could be caused by the numerous microcracks in the rock with plastic-elastic deformation characteristics. Under low normal stress, the internal damage of the rock accumulated continuously overtime and with the increasing shear stress. Damage occurred when the local damage reached the limit and lost the bearing capacity. Under high normal stress, the microcracks in the normal direction of the rock were compacted closely, thereby making the hardening effect caused by the compaction of microcracks more obvious than that under low stress. Meanwhile, under the condition of dense microfractures, the mechanical properties and internal continuity of the rock improved, thus strengthening the capability to transfer stress inside the rock, increasing the effective bearing area, and strengthening the capability to resist damage. Therefore, the ratio of long-term shear strength to fast shear strength of the rock under high normal stress is greater than that under low normal stress.

4. Improved Nonlinear Shear Creep Model Based on the Nishihara Model

The test results above illustrate that during the process of creep from the decay creep stage to the stable creep stage, the internal microcracks are continuously compacted, which causes irreversible plastic deformation and a hardening effect. Therefore, for rocks with an obvious hardening effect under low shear stress conditions, the traditional Nishihara model with linear parameters is no longer applicable. The model parameters must be described in a nonlinear manner. To reflect the mechanical properties of the rock in the creep process accurately, a time-varying factor was introduced to improve the traditional Nishihara model, and an improved variable-parameter nonlinear Nishihara shear creep model of rock was established. The rationality of the model was verified by the creep test result of specimens.

4.1. Description of the Characteristics of the Time-Dependent Parameter in the Nishihara Model. The Nishihara model is a rheological model composed of Hooke, Kelvin, and viscoplastic bodies in series, as shown in Figure 7. The model expression is

$$\gamma = \begin{cases} \dfrac{\tau}{G_M} + \dfrac{\tau}{G_K}\left(1 - e^{-(G_K/\eta_K)t}\right), & \tau < \tau_s, \\ \dfrac{\tau}{G_M} + \dfrac{\tau}{G_K}\left(1 - e^{-(G_K/\eta_K)t}\right) + \dfrac{\tau - \tau_s}{\eta_2}t, & \tau > \tau_s, \end{cases} \tag{2}$$

where G_M is the Hooke body coefficient, which is the instantaneous elastic modulus; G_K is the Kelvin model elastic coefficient; η_K is the Kelvin model viscosity coefficient; η_2 is the viscous element coefficient in the viscoplastic body; τ_s is the long-term shear strength of the rock; and t_s is the moment when the accelerated creep stage begins.

To describe the nonlinearity of parameters in the Nishihara model under shear loading, time-varying factor D was introduced to the Nishihara model by referring to the method of establishing fractional-derivative models [55], to describe the variation in element coefficients in the Nishihara model with time, and a nonlinear shear creep model with variable parameters was constructed (Figure 8).

A large number of studies have shown that the internal damage/hardening variable is closely related to time as an exponential function [56]. Therefore, on the basis of previous studies, the time-varying factor D is defined as

$$D = \mu e^{-\alpha t}, \tag{3}$$

where $D \in [0, 1]$; μ and α are material parameters representing the variation in element coefficients $\mu \in [-\infty, 1]$; and $\alpha \in [0, +\infty]$.

Compared with the nonlinear function in the fractional-derivative model, which describes the aging characteristics of the model parameters with only one parameter [55, 57], in this paper, the function D used to describe the nonlinear characteristics of model parameters has two parameters,

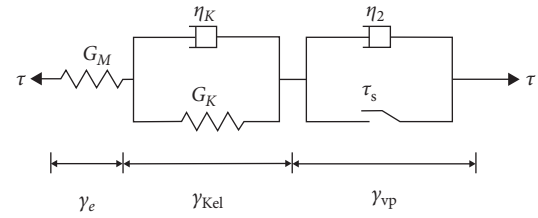

Figure 7: Nishihara rheological model.

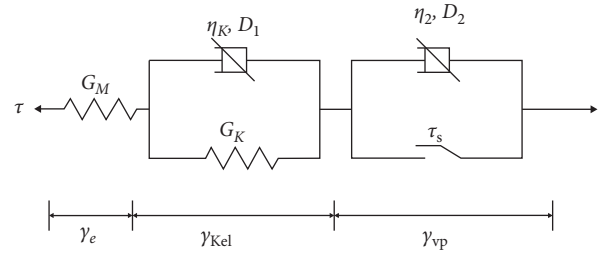

Figure 8: Improved nonlinear shear creep model with variable parameters.

where μ represents the comparison of model parameters before and after creep occurs, and α reflects the trend of the model parameters over time. It is not as simple and easy to calculate as the function in fractional-derivate models, but it can describe the evolution characteristics of model parameters during the creep process more comprehensively.

In the Nishihara model, the Kelvin body represents the attenuation and stable creep stages, and the viscoplastic body represents the accelerated creep stage. In the actual creep process, all parameters change with time. Time-varying factor D was introduced to the Kelvin and viscoplastic bodies to describe the relationship between the viscosity coefficient and time.

The Kelvin model is composed of an elastic element and a viscous element in parallel, and its constitutive equation is

$$\tau = \tau_1 + \tau_2 = G_K\gamma + \eta_K\dot{\gamma}, \tag{4}$$

$$\gamma = \gamma_1 = \gamma_2 = \frac{\tau_1}{G_K} = \frac{\tau_2}{\eta_K}t, \tag{5}$$

$$\gamma(t) = \frac{\tau}{G_K}\left(1 - e^{-(G_K/\eta_K)t}\right). \tag{6}$$

After introducing time-varying factor D, the Kelvin viscous element with variable parameters is expressed as

$$\eta_K^t = \eta_K^\infty(1 - D_1) = \eta_K^\infty\left(1 - \mu_1 e^{-\alpha_1 t}\right), \tag{7}$$

where η_K^t is the actual viscosity coefficient that changes over time, when $t = \infty$, $\eta_K^t = \eta_K^\infty$, η_K^∞ is the viscosity coefficient of the final moment of rock stable creep; μ_1 is the material parameter characterizing the damage/hardening degree of η_K; when μ_1 is positive, η_K hardens with time during rock creep; when $\mu_1 \longrightarrow 1$, η_K hardens into a plastomer at $t = \infty$; when $\mu_1 = 0$, η_K is constant, which is the original Kelvin model; when μ_1 is negative, η_K deteriorates with time during rock creep; when $\mu_1 \longrightarrow \infty$, η_K softens into an ideal fluid at

$t = \infty$; α_1 is a parameter reflecting the trend of η_K over time in the creep process; the larger α_1 is, the longer it takes for the η_K to stabilize.

Equation (7) indicates that when $t = 0$, the initial viscous element coefficient η_K^0 is

$$\eta_K^0 = \eta_K^\infty (1 - D_1) = \eta_K^\infty (1 - \mu_1). \tag{8}$$

In accordance with (3)–(7), the constitutive equation of nonlinear Kelvin model with parameter changes is obtained as follows:

$$\begin{aligned} \tau &= \tau_1 + \tau_2 = G_K + \eta_K^t \dot{\gamma}, \\ \eta_K^t \dot{\gamma} &= \eta_K^\infty \left(1 - \mu_1 e^{-\alpha_1 t}\right)\dot{\gamma} = \tau - G_K \gamma. \end{aligned} \tag{9}$$

Combined with the initial conditions $t = 0$ and $\gamma = 0$, the Kelvin nonlinear shear creep model equation with parameter variation is obtained as follows:

$$\gamma_{\text{kel}} = \frac{\tau}{G_K}\left(1 - e^{-\left(G_K/\eta_K^\infty\right)\left(\left(\ln\left(e^{\alpha_1 t} - \mu_1\right) - \ln\left(1 - \mu_1\right)\right)/\alpha_1\right)}\right). \tag{10}$$

Similarly, for the viscoplastic body introduced with time-varying factor D, the viscous element with variable parameters is expressed as

$$\eta_2^t = \eta_2^\infty (1 - D_2) = \eta_2^\infty \left(1 - \mu_2 e^{-\alpha_2 t}\right), \tag{11}$$

where η_2^t is the actual viscosity coefficient that changes over time, when $t = \infty$, $\eta_2^t = \eta_2^\infty$, η_2^∞ is the viscosity coefficient of the final moment of rock accelerated creep; when $\mu_2 > 0$, η_2 hardens with time, and the larger μ_2 represents the higher degree of hardening; when $\mu_2 < 0$, η_2 softens with time, and the smaller μ_2 represents the higher degree of softness.

The constitutive equation of viscoplastic body of Nishihara model is

$$\tau - \tau_s = \eta_2 \dot{\gamma}_{\text{vp}}. \tag{12}$$

Combining (11) and (12), the constitutive equation of the viscous element with variable parameters is obtained as follows:

$$\tau - \tau_s = \eta_2 (1 - D_2)\dot{\gamma}_{\text{vp}} = \eta_2\left(1 - \mu_2 \mathrm{e}^{-\alpha_2 (t - t_s)}\right)\dot{\gamma}_{\text{vp}}, \tag{13}$$

$$\gamma_{\text{vp}} = \frac{\tau - \tau_s}{\alpha_2 \eta_2} \ln\left(\mathrm{e}^{\alpha_2 (t - t_s)} - \mu_2\right). \tag{14}$$

Combining (10) and (14), the constitutive model of improved nonlinear Nishihara shear creep model with variable parameters can be obtained as follows:

$$\gamma(t) = \begin{cases} \dfrac{\tau}{G_M} + \dfrac{\tau}{G_K}\left(1 - e^{-\left(G_K/\eta_K^\infty\right)\left(\left(\ln\left(e^{\alpha_1 t} - \mu_1\right) - \ln\left(1 - \mu_1\right)\right)/\alpha_1\right)}\right), & \tau < \tau_s, \\ \dfrac{\tau}{G_M} + \dfrac{\tau}{G_K}\left(1 - e^{-\left(G_K/\eta_K^\infty\right)\left(\left(\ln\left(e^{\alpha_1 t} - \mu_1\right) - \ln\left(1 - \mu_1\right)\right)/\alpha_1\right)}\right) & \\ \quad + \dfrac{\tau - \tau_s}{\alpha_2 \eta_2^\infty} \ln\left(\mathrm{e}^{\alpha_2 (t - t_s)} - \mu_2\right), & \tau > \tau_s. \end{cases} \tag{15}$$

4.2. Model Verification. To test the correctness of the improved nonlinear shear creep model established in this study, the model was used to fit the test curve with the experimental data of specimens, which was compared with the fitting curve of the original Nishihara model to determine the advantages and disadvantages of the improved model. The parameters of the improved model are given in Table 3. The fitting results are shown in Figure 9, and it indicates that the improved Nishihara model was closer to the creep test curve than the original Nishihara model was, thereby reflecting the mechanical behavior of the specimen creep process and verifying the reasonableness of the model.

4.3. Relationship between Creep Model Parameters and Stress. In rock rheology, constitutive model parameters have important physical and mechanical significance. Studying the relationship between model parameters and loading conditions (stress, loading rate, etc.) can effectively reveal the mechanical mechanism of rock rheology [58–60]. In order to better understand the mechanical properties characterized by D, on the basis of Table 3, the relationship between μ_1, α_1, and shear stress under the normal stress 1.56 MPa is plotted in Figure 10. It could be seen from Figure 10 that μ_1 is greater than 0 under each shear stress condition, and the maximum value occurs when the shear stress is 1.68 MPa and then decreases with the increase of shear stress and finally stabilizes to 0.97, indicating that the nonlinear Kelvin viscosity coefficient has hardening under various shear stress conditions, and the hardening degree is the highest under low shear stress condition, and the hardening degree tends to be stable after shear stress increases. As shown in Figure 10, as the shear stress increases, α_1 increases first, then decays, and then continues to increase. Combined with (7), it can be seen that the time required for the viscosity coefficient in the nonlinear Kelvin body to reach stability is relatively long under the condition of low shear stress and then fluctuates with the increase of shear stress, but all remain stable at a certain value. Finally, when the shear stress reaches the value beyond the long-term strength, it decreases rapidly, and this phenomenon is caused by the compaction of rock-like specimen under low shear stress conditions. The relationship between η_K^t and time in accordance with (7) and Table 4 is plotted in Figure 11, which can better show the change process of η_K^t represented by μ_1 and α_1.

The relationship between Kelvin model elastic coefficient G_K and shear stress is plotted in Figure 12(b), and it shows that when the range of the shear stress was from 1.68 MPa to 2.24 MPa, Kelvin model elastic coefficient G_K increased with stress, and this result indicates the obvious internal hardening effect of the specimen and the characteristics of the plastic-elastic deformation of the rock-like specimen that not only hardens under low-stress fast shear but also under low-stress creep. When the shear stress was loaded to 2.8 MPa, the G_K was attenuated, indicating that under this shear stress condition, the internal microcracks of the specimen began to develop and damage began to occur. After the shear stress reached 3.36 MPa, the specimen

Table 3: Model parameters under various shear stresses conditions.

Normal stress (MPa)	Shear stress (MPa)	G_M (MPa)	G_K (MPa)	η_K^∞ (MPa·h)	η_2^∞ (MPa·h)	μ_1	α_1	τ_s (MPa)	t_s (h)	μ_2	α_2	Correlation coefficient R^2
0.78	1.23	0.8	11.60	44.866	—	0.985	3.861	—	—	—	—	0.998
	1.64	0.93	24.35	174.511	—	0.977	0.601	—	—	—	—	0.999
	2.05	1.01	22.36	137.981	—	0.996	1.096	—	—	—	—	0.997
	2.46	1.06	21.59	105.654	—	0.993	1.324	—	—	—	—	0.996
	2.87	1.08	19.67	196.583	—	0.991	0.703	—	—	—	—	0.999
1.56	1.68	1.06	17.58	260.98	—	0.999	0.435	—	—	—	—	0.999
	2.24	1.57	116.67	1212.06	—	0.977	0.628	—	—	—	—	0.999
	2.8	1.76	39.27	982.89	—	0.971	0.390	—	—	—	—	0.999
	3.36	0.74	7.10	3.9693	0.087	0.970	20.32	2.8	0.2634	−14.70	3.64	0.996
2.34	1.935	1.16	17.06	37.564	—	0.984	3.868	—	—	—	—	0.998
	2.58	1.26	32.09	1223.15	—	0.983	0.145	—	—	—	—	0.997
	3.87	1.48	42.2	603.86	—	0.990	0.787	—	—	—	—	0.999
	4.515	1.55	17.94	291.13	—	0.986	0.461	—	—	—	—	0.996
	5.16	1.57	9.52	245.49	—	0.977	0.192	—	—	—	—	0.998
3.12	2.199	0.54	22.15	212.33	—	0.993	1.894	—	—	—	—	0.999
	2.99	0.65	22.46	370.49	—	0.979	0.246	—	—	—	—	0.998
	4.398	0.86	25.86	287.12	—	0.997	0.769	—	—	—	—	0.997
	5.131	0.97	21.73	186.73	—	0.999	1.678	—	—	—	—	0.999
	5.864	1.06	21.76	290.39	—	0.999	0.821	—	—	—	—	0.998

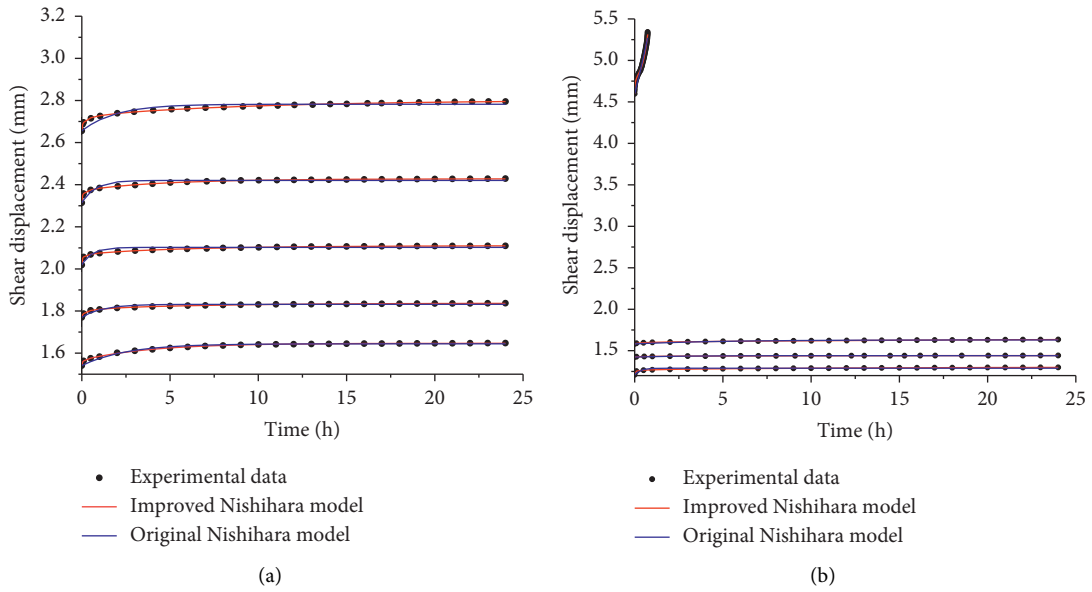

Figure 9: Continued.

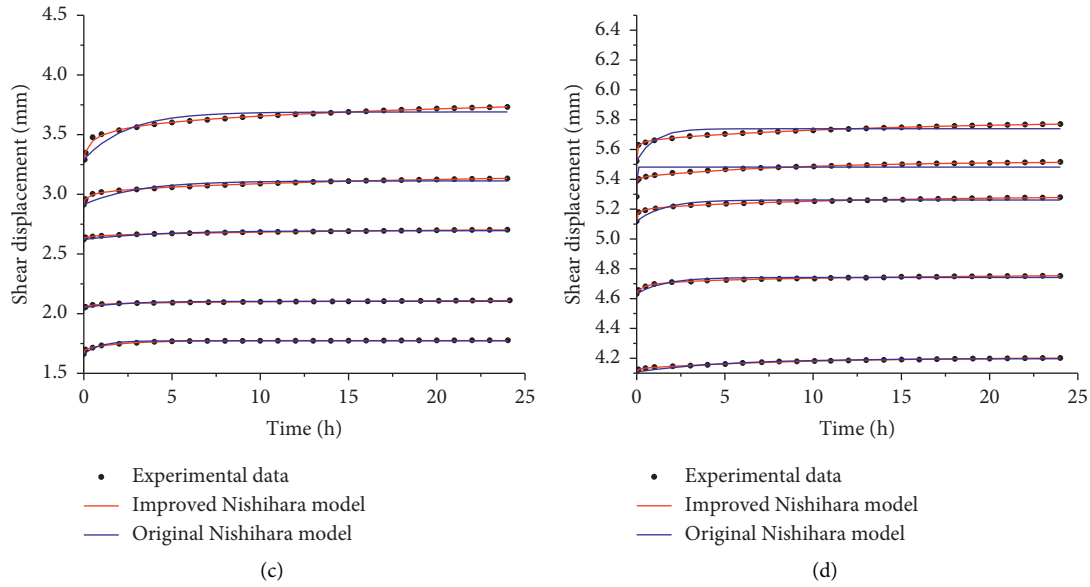

Figure 9: Comparison of the test and calculated values of the creep model under normal stress (a) 0.78 MPa, (b) 1.56 MPa, (c) 2.34 MPa, and (d) 3.12 MPa.

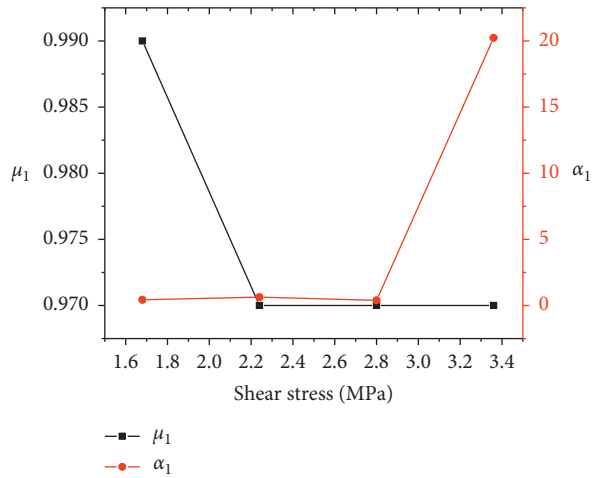

Figure 10: The relationship between $\mu 1$, $\alpha 1$, and shear stress diagram.

Table 4: Initial viscosity coefficient η_0 under different shear stress conditions.

Shear stress (MPa)	1.68	2.24	2.8	3.36
η_0 (MPa·h)	23.56	67.65	46.84	0.098

quickly entered the accelerated creep stage. The viscosity parameter of the viscous element in the viscoplastic body that describes the accelerated creep stage was negative, indicating that the internal damage of the specimen was continuously intensified and the creep rate was continuously accelerated until failure.

4.4. Long-Term Strength Determination Method Based on Improved Nonlinear Model. It can be concluded from (10) that the rock-like specimen creep deformation is controlled by G_K; when G_K is small, the mass of rock creep deformation is large; that is, the larger G_K is, the smaller the creep deformation is. G_K characterizes the ability to resist creep deformation. Therefore, in the improved nonlinear model, the author proposes a method to determine the long-term strength by using the curve of G_K-shear stress. This method uses the nonlinear Nishihara model proposed in this paper to fit shear displacement-time curve to obtain the curve of $G_K - \tau$ and then determines the shear stress of G_K decay in the curve as the long-term strength. According to the parameters in Table 3, the $G_K - \tau$ curves of the specimen under different

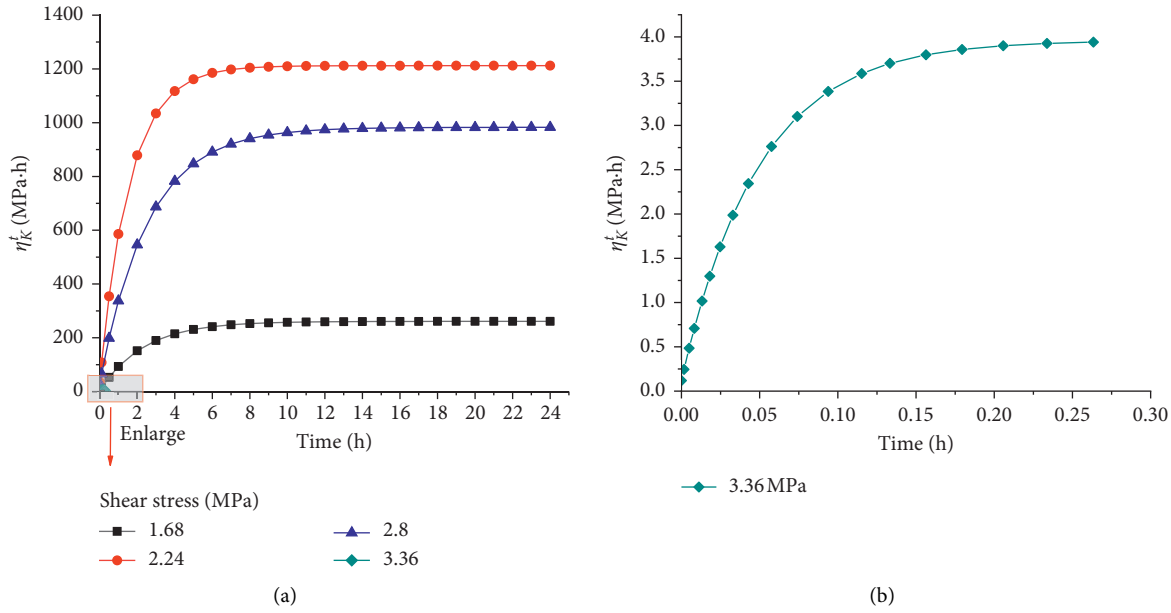

Figure 11: The relationship between η_K^t and time diagram.

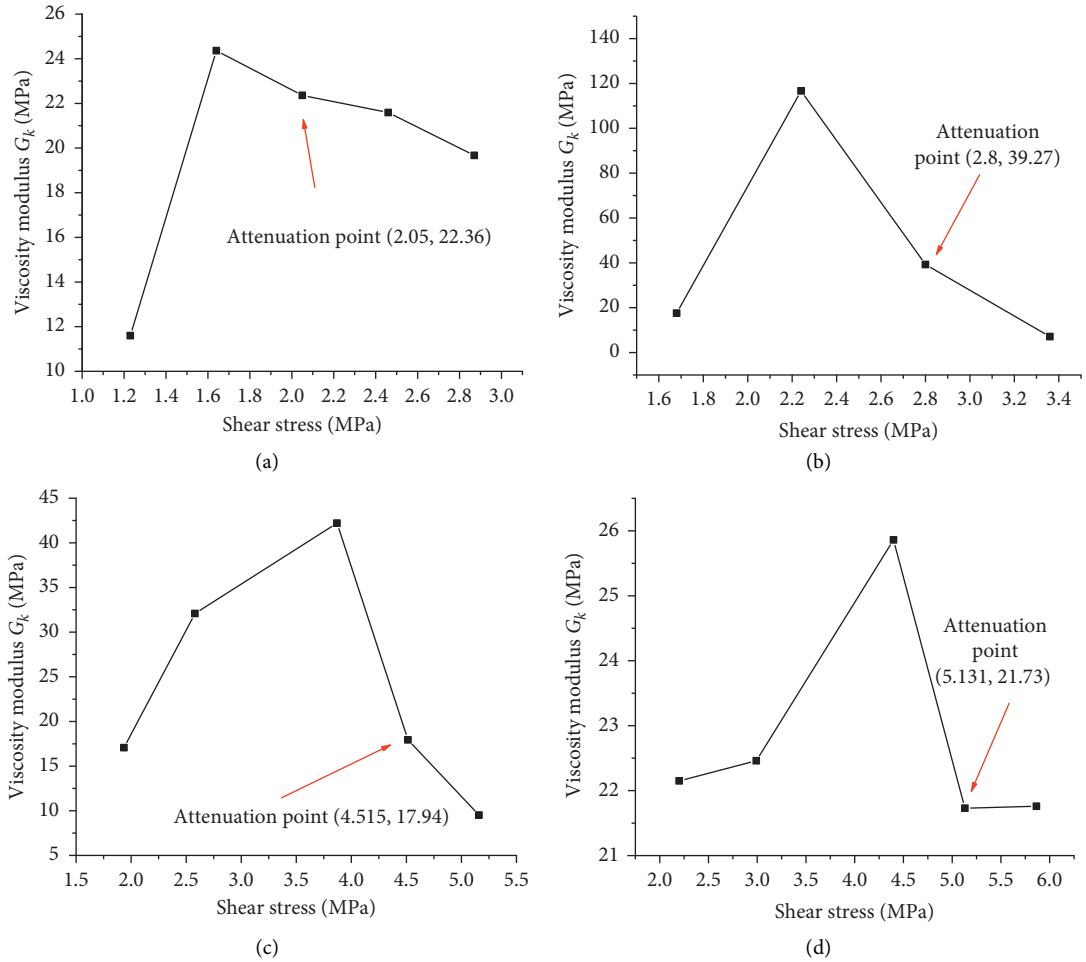

Figure 12: The relationship between viscosity modulus G_K-shear stress diagram under normal stress (a) 0.78 MPa, (b) 1.56 MPa, (c) 2.34 MPa, and (d) 3.12 MPa.

Table 5: Comparison of two methods for determining long-term shear strength.

Specimen number	Normal stress (MPa)	Long-term shear stress (MPa)	
		Isochronous curve method	Modulus inflection point method
1	0.78	2.04	2.04
2	1.56	2.8	2.8
3	2.34	4.515	4.515
4	3.12	5.131	5.131

normal stress levels were drawn (Figure 12) and were compared with the long-term shear strength determined by the isochronous curve method, as shown in Table 5.

Table 5 shows that the long-term shear strength determined by these two methods is basically the same, which proves the effectiveness of the long-term strength determination method proposed in this paper. And compared with the isochronous curve method, the modulus inflection point method only needs to fit the experimental data to determine the G_K under each stress condition. Then, the long-term strength of the rock can be obtained according to the attenuation of G_K, which has a simpler and faster operation process.

5. Discussion and Conclusion

Research on the mechanical characteristics of plastic-elastic rock deformation under the conditions of fast shear and shear creep indicates that under low shear stress, the mechanical properties of rocks with plastic-elastic deformation are continuously strengthened during creep, thereby continuously enhancing the rock's resistance to deformation. When the shear stress level increases, the microcracks inside the rock are completely compacted. At this time, the mechanical properties of the rock deteriorate with creep and aging. Meanwhile, the mechanical properties of rocks with plastic-elastic deformation under different normal stress conditions differ. The rock bearing capacity and the damage resistance under high normal stress are better than those under low normal stress. Therefore, for rock mass engineering, the rock with plastic-elastic deformation characteristics should be placed under low stress conditions, and the surrounding area should avoid high-intensity stress field to enhance the stability of the engineering and the project.

In this work, a time-varying factor D was introduced to describe the viscous elements in a nonlinear manner, and an improved nonlinear shear creep model based on the Nishihara model was established. After fitting the experimental data, it is found that the model can reflect the shear creep behavior of rock-like specimens effectively, and the model has rationality. In addition, under the normal stress of 0.78 MPa and 1.56 MPa, the ratio of long-term shear strength to fast shear strength of rock samples with plastic-elastic deformation characteristics is 0.5, indicating that the critical damage cumulative value required for rock reaches a failure state. Therefore, in a project, the long-term shear strength at which the cracks inside the rock begin to develop and expand must be determined to prevent rock destruction. At present, relevant scholars often monitor rock damage under creep conditions by calculating the creep rate, the deformation modulus, or the monitoring energy of the acoustic emission equipment. However, in practical engineering, calculating the rate at each moment or providing special equipment is difficult. By fitting the improved nonlinear Nishihara shear creep model to the surrounding rock displacement-time data monitored in the project, the damage can be discriminated according to the identified trend of the viscous modulus G_k of the surrounding rock so as to provide timely support and avoid the structural instability of the project, which is crucial in practical engineering. Furthermore, according to the fact that G_k of the nonlinear model can characterize the creep deformation resistance of rock-like specimen, a method to determine the long-term shear strength is proposed, and compared with the calculation results of isochronous curve method, the rationality and applicability of the method are verified.

Notations

σ_c: Uniaxial compressive strength
μ: Poisson's ratio
φ: Angle of internal friction
c: Cohesive force
E: The deformation modulus
τ_1, τ_2: Adjacent two-stage shear stress
$\gamma_{\tau 1}^t, \gamma_{\tau 2}^t$: The shear displacement at different moments
G_M: The Hooke body coefficient
G_K: The Kelvin model elastic coefficient
η_K: The Kelvin model viscosity coefficient
η_2: The viscous element coefficient in the viscoplastic body
τ_s: The long-term shear strength of the rock
t_s: The moment when the accelerated creep stage begins
μ, α: Material parameters representing the variation in element coefficients
η_K^∞: The element coefficient after entering the stable creep stage
η_K^t: The real-time element coefficient
μ_1, α_1: Material parameters representing the variation in Kelvin model element coefficients
μ_2, α_2: Material parameters representing the variation in viscoplastic body element coefficients
τ_s: The long-term strength of the rock.

Data Availability

All data generated or analyzed during this study are included in this article.

Conflicts of Interest

The authors declare that they have no conflicts of interest.

Acknowledgments

This work was supported by the National Natural Science Foundation of China (51774322, 51774107, and 51774131), Hunan Provincial Natural Science Foundation of China (2018JJ2500), and Fundamental Research Funds for the Central Universities of Central South University (2019zzts669). The authors wish to acknowledge these supports.

References

[1] O. Hamza and R. Stace, "Creep properties of intact and fractured muddy siltstone," *International Journal of Rock Mechanics and Mining Sciences*, vol. 106, pp. 109–116, 2018.

[2] A. Sainoki, S. Tabata, H. S. Mitri, D. Fukuda, and J.-I. Kodama, "Time-dependent tunnel deformations in homogeneous and heterogeneous weak rock formations," *Computers and Geotechnics*, vol. 92, pp. 186–200, 2017.

[3] P. Cao, Y. Wen, Y. Wang, H. Yuan, and B. Yuan, "Study on nonlinear damage creep constitutive model for high-stress soft rock," *Environmental Earth Sciences*, vol. 75, p. 900, 2016.

[4] Y. Zhao, Y. Wang, W. Wang, W. Wan, and J. Tang, "Modeling of non-linear rheological behavior of hard rock using triaxial rheological experiment," *International Journal of Rock Mechanics and Mining Sciences*, vol. 93, pp. 66–75, 2017.

[5] C. Jiang, Z. Zhang, and J. He, "Nonlinear analysis of combined loaded rigid piles in cohesionless soil slope," *Computers and Geotechnics*, vol. 117, p. 103225, 2020.

[6] K. Hu, F. Qian, H. Li, and Q. Hu, "Study on creep characteristics and constitutive model for thalam rock mass with fracture in tunnel," *Geotechnical & Geological Engineering*, vol. 36, pp. 827–834, 2017.

[7] Q. Zhang, M. Shen, W. Ding, and C. Clark, "Shearing creep properties of cements with different irregularities on two surfaces," *Journal of Geophysics and Engineering*, vol. 9, no. 2, pp. 210–217, 2012.

[8] S. N. Moghadam, K. Nazokkar, R. J. Chalaturnyk, and H. Mirzabozorg, "Parametric assessment of salt cavern performance using a creep model describing dilatancy and failure," *International Journal of Rock Mechanics and Mining Sciences*, vol. 79, pp. 250–267, 2015.

[9] Y. Zhao, L. Zhang, W. Wang et al., "Creep behavior of intact and cracked limestone under multi-level loading and unloading cycles," *Rock Mechanics & Rock Engineering*, vol. 50, no. 6, pp. 1409–1424, 2017.

[10] Z.-L. He, Z.-D. Zhu, X.-H. Ni, and Z.-J. Li, "Shear creep tests and creep constitutive model of marble with structural plane," *European Journal of Environmental and Civil Engineering*, vol. 23, no. 11, pp. 1275–1293, 2017.

[11] L. Yang and Z.-D. Li, "Nonlinear variation parameters creep model of rock and parametric inversion," *Geotechnical and Geological Engineering*, vol. 36, no. 5, pp. 2985–2993, 2018.

[12] H. Mansouri and R. Ajalloeian, "Mechanical behavior of salt rock under uniaxial compression and creep tests," *International Journal of Rock Mechanics and Mining Sciences*, vol. 110, pp. 19–27, 2018.

[13] A. Fahimifar, M. Karami, and A. Fahimifar, "Modifications to an elasto-visco-plastic constitutive model for prediction of creep deformation of rock samples," *Soils and Foundations*, vol. 55, no. 6, pp. 1364–1371, 2015.

[14] H. Özşen, İ Özkan, and C. Şensöğüt, "Measurement and mathematical modelling of the creep behaviour of Tuzköy rock salt," *International Journal of Rock Mechanics & Mining Sciences*, vol. 66, pp. 128–135, 2014.

[15] A. Singh, C. Kumar, L. G. Kannan, K. S. Rao, and R. Ayothiraman, "Estimation of creep parameters of rock salt from uniaxial compression tests," *International Journal of Rock Mechanics and Mining Sciences*, vol. 107, pp. 243–248, 2018.

[16] C. C. Xia, L. Jin, and R. Guo, "Nonlinear theoretical rheological model for rock: a review and some problems," *Chinese Journal of Rock Mechanics and Engineering*, vol. 30, no. 3, pp. 453–463, 2011.

[17] L. Liu, G.-M. Wang, J.-H. Chen, and S. Yang, "Creep experiment and rheological model of deep saturated rock," *Transactions of Nonferrous Metals Society of China*, vol. 23, no. 2, pp. 478–483, 2013.

[18] F. Deleruyelle, T. A. Bui, H. Wong, N. Dufour, D. K. Tran, and X. S. Zhang, "Analytical study of the post-closure behaviour of a deep tunnel in a porous creeping rock mass," *Comptes Rendus Mécanique*, vol. 344, no. 9, pp. 649–660, 2016.

[19] C. Y. Zhang, H. Lin, C. M. Qiu, T. T. Jiang, and J. H. Zhang, "The effect of cross-section shape on deformation, damage and failure of rock-like materials under uniaxial compression from both a macro and micro viewpoint," *International Journal of Damage Mechanics*, vol. 20, pp. 1–20, 2020.

[20] X. H. Xu, S. P. Ma, M. F. Xia, F. J. Ke, and Y. L. Bai, "Damage evaluation and damage localization of rock," *Theoretical and Applied Fracture Mechanics*, vol. 42, no. 2, pp. 131–138, 2004.

[21] S. P. Jia, L. W. Zhang, B. S. Wu, H. D. Yu, and J. X. Shu, "A coupled hydro-mechanical creep damage model for clayey rock and its application to nuclear waste repository," *Tunnelling and Underground Space Technology*, vol. 74, pp. 230–246, 2018.

[22] S. N. Moghadamaab, "Modeling time-dependent behavior of gas caverns in rock salt considering creep, dilatancy and failure," *Tunnelling & Underground Space Technology*, vol. 33, pp. 171–185, 2013.

[23] J. F. Shao, Q. Z. Zhu, and K. Su, "Modeling of creep in rock materials in terms of material degradation," *Computers and Geotechnics*, vol. 30, no. 7, pp. 549–555, 2003.

[24] H. Lin, X. Ding, R. Yong, W. Xu, and S. Du, "Effect of non-persistent joints distribution on shear behavior," *Comptes Rendus Mécanique*, vol. 347, no. 6, pp. 477–489, 2019.

[25] Y. Shen, Y. Wang, Y. Yang, Q. Sun, T. Luo, and H. Zhang, "Influence of surface roughness and hydrophilicity on bonding strength of concrete-rock interface," *Construction and Building Materials*, vol. 213, pp. 156–166, 2019.

[26] D. Lei, H. Lin, Y. Chen, R. Cao, and Z. Wen, "Effect of cyclic freezing-thawing on the shear mechanical characteristics of nonpersistent joints," *Advances in Materials Science and Engineering*, vol. 2019, Article ID 9867681, 14 pages, 2019.

[27] C. Zhang, C. Pu, R. Cao, T. Jiang, and G. Huang, "The stability and roof-support optimization of roadways passing through unfavorable geological bodies using advanced detection and monitoring methods, among others, in the Sanmenxia Bauxite Mine in China's Henan Province," *Bulletin of Engineering Geology and the Environment*, vol. 78, no. 7, pp. 5087–5099, 2019.

[28] J. Jin, P. Cao, Y. Chen, C. Pu, D. Mao, and X. Fan, "Influence of single flaw on the failure process and energy mechanics of rock-like material," *Computers and Geotechnics*, vol. 86, pp. 150–162, 2017.

[29] Y. Chen and H. Lin, "Consistency analysis of Hoek-Brown and equivalent Mohr-coulomb parameters in calculating slope safety factor," *Bulletin of Engineering Geology and the Environment*, vol. 78, no. 6, pp. 4349–4361, 2019.

[30] H. Lin, Y. Zhu, J. Yang, and Z. Wen, "Anchor stress and deformation of the bolted joint under shearing," *Advances in Civil Engineering*, vol. 2020, Article ID 3696489, 10 pages, 2020.

[31] X.-Y. Yu, T. Xu, M. Heap, G.-L. Zhou, and P. Baud, "Numerical approach to creep of rock based on the numerical manifold method," *International Journal of Geomechanics*, vol. 18, no. 11, Article ID 04018153, 2018.

[32] H. W. Zhou, C. P. Wang, B. B. Han, and Z. Q. Duan, "A creep constitutive model for salt rock based on fractional derivatives," *International Journal of Rock Mechanics and Mining Sciences*, vol. 48, no. 1, pp. 116–121, 2011.

[33] M.-D. Wei, F. Dai, J.-W. Zhou, Y. Liu, and J. Luo, "A further improved maximum tangential stress criterion for assessing mode I fracture of rocks considering non-singular stress terms of the Williams expansion," *Rock Mechanics and Rock Engineering*, vol. 51, no. 11, pp. 3471–3488, 2018.

[34] G. Chen, T. Chen, Y. Chen, R. Huang, and M. Liu, "A new method of predicting the prestress variations in anchored cables with excavation unloading destruction," *Engineering Geology*, vol. 241, pp. 109–120, 2018.

[35] Y. Chen and C. C. Li, "Performance of fully encapsulated rebar bolts and D-Bolts under combined pull-and-shear loading," *Tunnelling and Underground Space Technology*, vol. 45, pp. 99–106, 2015.

[36] Y. Zhao, Y. Wang, W. Wang, L. Tang, Q. Liu, and G. Cheng, "Modeling of rheological fracture behavior of rock cracks subjected to hydraulic pressure and far field stresses," *Theoretical and Applied Fracture Mechanics*, vol. 101, pp. 59–66, 2019.

[37] Y. Zhao, L. Zhang, W. Wang, C. Pu, W. Wan, and J. Tang, "Cracking and stress-strain behavior of rock-like material containing two flaws under uniaxial compression," *Rock Mechanics and Rock Engineering*, vol. 49, no. 7, pp. 2665–2687, 2016.

[38] H. Chen, X. Fan, H. Lai, Y. Xie, and Z. He, "Experimental and numerical study of granite blocks containing two side flaws and a tunnel-shaped opening," *Theoretical and Applied Fracture Mechanics*, vol. 104, Article ID 102394, 2019.

[39] Y. Wang, H. Zhang, H. Lin, Y. Zhao, and Y. Liu, "Fracture behaviour of central-flawed rock plate under uniaxial compression," *Theoretical and Applied Fracture Mechanics*, vol. 106, Article ID 102503, 2020.

[40] F. Dai, M. D. Wei, N. W. Xu, Y. Ma, and D. S. Yang, "Numerical assessment of the progressive rock fracture mechanism of cracked chevron notched Brazilian disc specimens," *Rock Mechanics and Rock Engineering*, vol. 48, no. 2, pp. 463–479, 2015.

[41] H.-B. Du, F. Dai, Y. Xu, Z. Yan, and M.-D. Wei, "Mechanical responses and failure mechanism of hydrostatically pressurized rocks under combined compression-shear impacting," *International Journal of Mechanical Sciences*, vol. 165, Article ID 105219, 2020.

[42] C. C. Xia and Z. Q. Sun, *Engineering Rock Joint Mechanics*, Tongji Press, Shanghai, China, 2002.

[43] S. Xie, H. Lin, Y. Wang et al., "A statistical damage constitutive model considering whole joint shear deformation," *International Journal of Damage Mechanics*, vol. 29, Article ID 105678951990077, 2020.

[44] X. Fan, H. Lin, H. Lai, R. Cao, and J. Liu, "Numerical analysis of the compressive and shear failure behavior of rock containing multi-intermittent joints," *Comptes Rendus Mécanique*, vol. 347, no. 1, pp. 33–48, 2019.

[45] H. Lin, H. Yang, Y. Wang, Y. Zhao, and R. Cao, "Determination of the stress field and crack initiation angle of an open flaw tip under uniaxial compression," *Theoretical and Applied Fracture Mechanics*, vol. 104, Article ID 102358, 2019.

[46] Y. Wang, H. Lin, Y. Zhao, X. Li, P. Guo, and Y. Liu, "Analysis of fracturing characteristics of unconfined rock plate under edge-on impact loading," *European Journal of Environmental and Civil Engineering*, vol. 23, pp. 1–16, 2019.

[47] Y.-H. Huang, S.-Q. Yang, P. G. Ranjith, and J. Zhao, "Strength failure behavior and crack evolution mechanism of granite containing pre-existing non-coplanar holes: experimental study and particle flow modeling," *Computers and Geotechnics*, vol. 88, pp. 182–198, 2017.

[48] S.-Q. Yang, X.-R. Liu, and H.-W. Jing, "Experimental investigation on fracture coalescence behavior of red sandstone containing two unparallel fissures under uniaxial compression," *International Journal of Rock Mechanics and Mining Sciences*, vol. 63, pp. 82–92, 2013.

[49] E. M. Gell, S. M. Walley, and C. H. Braithwaite, "Review of the validity of the use of artificial specimens for characterizing the mechanical properties of rocks," *Rock Mechanics and Rock Engineering*, vol. 52, no. 9, pp. 2949–2961, 2019.

[50] G. Wang, L. Zhang, Y. Zhang, and G. Ding, "Experimental investigations of the creep-damage-rupture behaviour of rock salt," *International Journal of Rock Mechanics and Mining Sciences*, vol. 66, pp. 181–187, 2014.

[51] C. Müller, T. Frühwirt, D. Haase, R. Schlegel, and H. Konietzky, "Modeling deformation and damage of rock salt using the discrete element method," *International Journal of Rock Mechanics and Mining Sciences*, vol. 103, pp. 230–241, 2018.

[52] H. Lin, S. Xie, R. Yong, Y. Chen, and S. Du, "An empirical statistical constitutive relationship for rock joint shearing considering scale effect," *Comptes Rendus Mécanique*, vol. 347, no. 8, pp. 561–575, 2019.

[53] R.-H. Cao, P. Cao, H. Lin, X. Fan, C. Zhang, and T. Liu, "Crack initiation, propagation, and failure characteristics of jointed rock or rock-like specimens: a review," *Advances in Civil Engineering*, vol. 2019, Article ID 6975751, 31 pages, 2019.

[54] S. Zhang, W. Liu, and H. Lv, "Creep energy damage model of rock graded loading," *Results in Physics*, vol. 12, pp. 1119–1125, 2019.

[55] H. Khajehsaeid, "A comparison between fractional-order and integer-order differential finite deformation viscoelastic models: effects of filler content and loading rate on material parameters," *International Journal of Applied Mechanics*, vol. 10, no. 9, Article ID 1850099, 2018.

[56] R. B. Wang, W. Y. Xu, W. Wang, and J. C. Zhang, "A nonlinear creep damage model for brittle rocks based on time-dependent damage," *European Journal of Environmental and Civil Engineering*, vol. 17, no. sup1, pp. s111–s125, 2013.

[57] C. Zopf, S. E. Hoque, and M. Kaliske, "Comparison of approaches to model viscoelasticity based on fractional time derivatives," *Computational Materials Science*, vol. 98, pp. 287–296, 2015.

[58] A. S. Khan, O. Lopez-Pamies, and R. Kazmi, "Thermo-mechanical large deformation response and constitutive modeling of viscoelastic polymers over a wide range of strain rates and temperatures," *International Journal of Plasticity*, vol. 22, no. 4, pp. 581–601, 2006.

[59] H. Khajehsaeid, S. Reese, J. Arghavani, and R. Naghdabadi, "Strain and stress concentrations in elastomers at finite deformations: effects of strain-induced crystallization, filler reinforcement, and deformation rate," *Acta Mechanica*, vol. 227, no. 7, pp. 1969–1982, 2016.

[60] H. Khajehsaeid, "Modeling nonlinear viscoelastic behavior of elastomers using a micromechanically motivated rate-dependent approach for relaxation times involved in integral-based models," *Constitutive Models for Rubber IX*, CRC Press, Boca Raton, FL, USA, pp. 181–188, 2015.